Quantification of Human Brain White Matter Myelination using ViSTa MRI Fingerprinting

Jialan Zheng[1,2], Cong Yang[3], Wen Zhong[1], Haoxiang Li[1], Ziang Wang[4], Xiaozhi Cao[5], Congyu Liao[5], Qiyuan Tian[1,3]

[1] School of Biomedical Engineering, Tsinghua University, Beijing, China;

[2] Tanwei College, Tsinghua University, Beijing, China;

[3] Tsinghua Laboratory of Brain and Intelligence, Tsinghua University, Beijing, China.

[4] Tsinghua Medicine, Tsinghua University, Beijing, China

[5] Department of Radiology, Stanford University, Stanford, CA, United States

Introduction

Myelination is crucial for neuronal signal transmission and indicates brain development and function. Various MRI techniques, like multi-compartment T2 mapping, magnetization transfer, and ViSTa method were used to study myelination (Piredda, 2021). Nonetheless, most previous studies focused on long-range association fibers (LAFs) in deep white matter (DWM), overlooking short-range association fibers (SAFs) in superficial white matter (SWM).

This study employs the advanced ViSTa-MR fingerprinting (MRF) sequence (Liao, 2023) in combination with diffusion and T1w sequences to assess myelin water fraction (MWF) and microstructural parameters from the Neurite Orientation Dispersion and Density Imaging (NODDI) model (Zhang, 2012). MWF and NODDI parameters are used to calculate the g-ratio (Stikov, 2015) that reflects relative myelin thickness, aiming to enhance our understanding of brain's structural and functional organization.

Method

Data. With written consent forms and IRB approval, T1w-MPRAGE, diffusion MRI and ViSTa-MRF data were acquired on 10 healthy young adults on a 3-Tesla scanner (Siemens, MAGNETOM Prisma) equipped with a 32-channel head coil. Diffusion data were acquired using a product 2D SMS-PGSE single-shot EPI sequence with 32 and 64 uniform directions at b=1000 and 2500 s/mm^2, respectively.

Processing. Freesurfer was used for cortical reconstruction and segmentation of T1w data (Fischl, 2012). The diffusion data were preprocessed using “topup” and “eddy” function from FSL (Smith, 2004). NODDI parameters were derived using inventors’ MATLAB toolbox. Multi-modal data were coregistered using Boundary-Based Registration (Douglas, 2009). G-ratio was calculated as described in Figure 1(A).

ROI extraction. ROIs for 42 deep white matter tracts were extracted by registering diffusion data to FSL xtract atlas in the MNI space. Whole-brain tractography was conducted using

MSMT-CSD (Jeurissen, 2014) and iFOD2 methods with (Tournier, 2010) SIFT correction. Voxels for LAFs and SAFs between any two cortical regions were extracted.

Statistics. MWF and g-ratio results were averaged across DWM tract voxels, and across cortical vertices, SAF and LAF voxels and subjects (then displayed on cortical surface). The correlation of the mean MWF, g-ratio and connectivity strength between any two cortices, along with the mean value of other imaging parameters of the two cortices were computed.

Result

Validation. Mean MWFs were projected to middle cortical surface (Figure 2A), showing higher myelination in primary motor, sensory, visual and auditory region, following expected anatomy and demonstrating validity of MWFs.

DWM tracts. Mean MWF and g-ratio values were depicted for each DWM tract (Figure 1B, 1C). Tracts like cingulum, AC and UF exhibit low MWF. FX tract exhibits low MWF and g-ratio, suggesting thinner axons. CST exhibits high MWF and g-ratio, indicating thicker axons. OR, AF, FMA, and FMI tracts show high MWF.

Association Fibers. Figure 2C shows comparison of myelination in association fibers between cortical regions. LAFs exhibit higher myelination than SAFs. SAFs under entorhinal cortex, parahippocampal region and temporal pole exhibit lower MWFs. SAFs from posterior cingulate show higher MWF. Figure 2B shows connectivity strength is negatively correlated with MWF (yellow box), whereas cortical volume and curvature are positively correlated with MWF (green box).

Conclusion

In DWM, myelination in fibers relevant to higher cognitive function is relatively low. Commissural fibers show higher myelination. Additionally, the spatial pattern of the myelination of the association fibers indicates the balance of connectivity strength and myelination.

Reference

1. Fischl, B. (2012). FreeSurfer. *NeuroImage, 62*(2), 774–781.
2. Greve, D. N., & Fischl, B. (2009). Accurate and robust brain image alignment using boundary-based registration. *NeuroImage, 48*(1), 63–72.
3. Jeurissen, B., Tournier, J.-D., Dhollander, T., Connelly, A., & Sijbers, J. (2014). Multi-tissue constrained spherical deconvolution for improved analysis of multi-shell diffusion MRI data. *NeuroImage, 103*, 411–426.
4. Liao, C., Cao, X., Iyer, S. S., Schauman, S., Zhou, Z., Yan, X., Chen, Q., Li, Z., Wang, N.,

Gong, T., Wu, Z., He, H., Zhong, J., Yang, Y., Kerr, A., Grill-Spector, K., & Setsompop, K. (2024). High-resolution myelin-water fraction and quantitative relaxation mapping using 3D ViSTa-MR fingerprinting. *Magnetic Resonance in Medicine, 91*(6), 2278–2293.

5. Piredda, G. F., Hilbert, T., Thiran, J.-P., & Kober, T. (2021). Probing myelin content of the human brain with MRI: A review. *Magnetic Resonance in Medicine, 85*(2), 627–652.

6. Smith, R. E., Tournier, J.-D., Calamante, F., & Connelly, A. (2013). SIFT: Spherical-deconvolution informed filtering of tractograms. NeuroImage, 67, 298–312.

7. Smith, S. M., Jenkinson, M., Woolrich, M. W., Beckmann, C. F., Behrens, T. E. J., Johansen-Berg, H., Bannister, P. R., De Luca, M., Drobnjak, I., Flitney, D. E., Niazy, R. K., Saunders, J., Vickers, J., Zhang, Y., De Stefano, N., Brady, J. M., & Matthews, P. M. (2004). Advances in functional and structural MR image analysis and implementation as FSL. *NeuroImage, 23*(Suppl 1), S208–S219.

8. Stikov, N., Campbell, J. S. W., Stroh, T., Lavelée, M., Frey, S., Novek, J., Nuara, S., Ho, M.-K., Bedell, B. J., Dougherty, R. F., Leppert, I. R., Boudreau, M., Narayanan, S., Duval, T., Cohen-Adad, J., Picard, P.-A., Gasecka, A., Côté, D., & Pike, G. B. (2015). In vivo histology of the myelin g-ratio with magnetic resonance imaging. *NeuroImage, 118*, 397–405.

9. Tournier, J.-D., Calamante, F., & Connelly, A. (2010). Improved probabilistic streamlines tractography by 2nd order integration over fibre orientation distributions. *Proceedings of the International Society for Magnetic Resonance in Medicine*, 1670.

10. Zhang, H., Schneider, T., Wheeler-Kingshott, C. A., & Alexander, D. C. (2012). NODDI: Practical in vivo neurite orientation dispersion and density imaging of the human brain. *NeuroImage, 61*(4), 1000–1016.

Figures

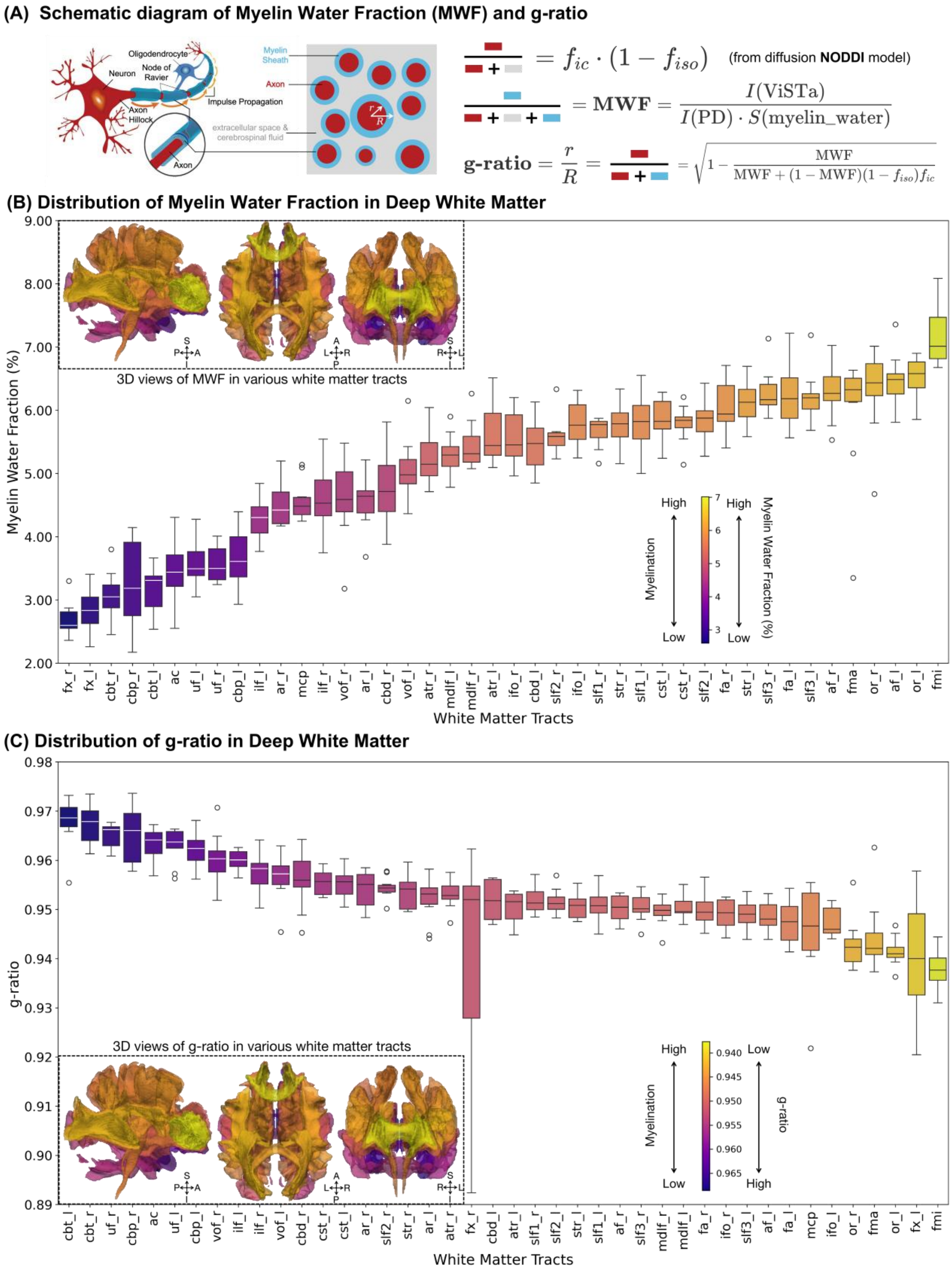

Figure 1. Spatial Analysis of Deep White Matter Myelination using Myelin Water Fraction and g-ratio. *Abbreviation: af=Arcuate Fasciculus; ar=Acoustic Radiation; atr=Anterior Thalamic Radiation; cbd=Cingulum subsection : Dorsal; cbp=Cingulum subsection : Peri-genual; cbt=Cingulum subsection : Temporal; cst=Corticospinal Tract ; fa=Frontal Aslant; fma=Forceps Major; fmi=Forceps Minor; fx=Fornix; ilf=Inferior Longitudinal Fasciculus; ifo=Inferior Fronto-Occipital Fasciculus; mcp=Middle Cerebellar Peduncle; mdlf=Middle Longitudinal Fasciculus; or=Optic Radiation; str=Superior Thalamic Radiation; slf=Superior Longitudinal Fasciculus; ac=Anterior Commissure; uf=Uncinate Fasciculus; vof=Vertical Occipital Fasciculus*

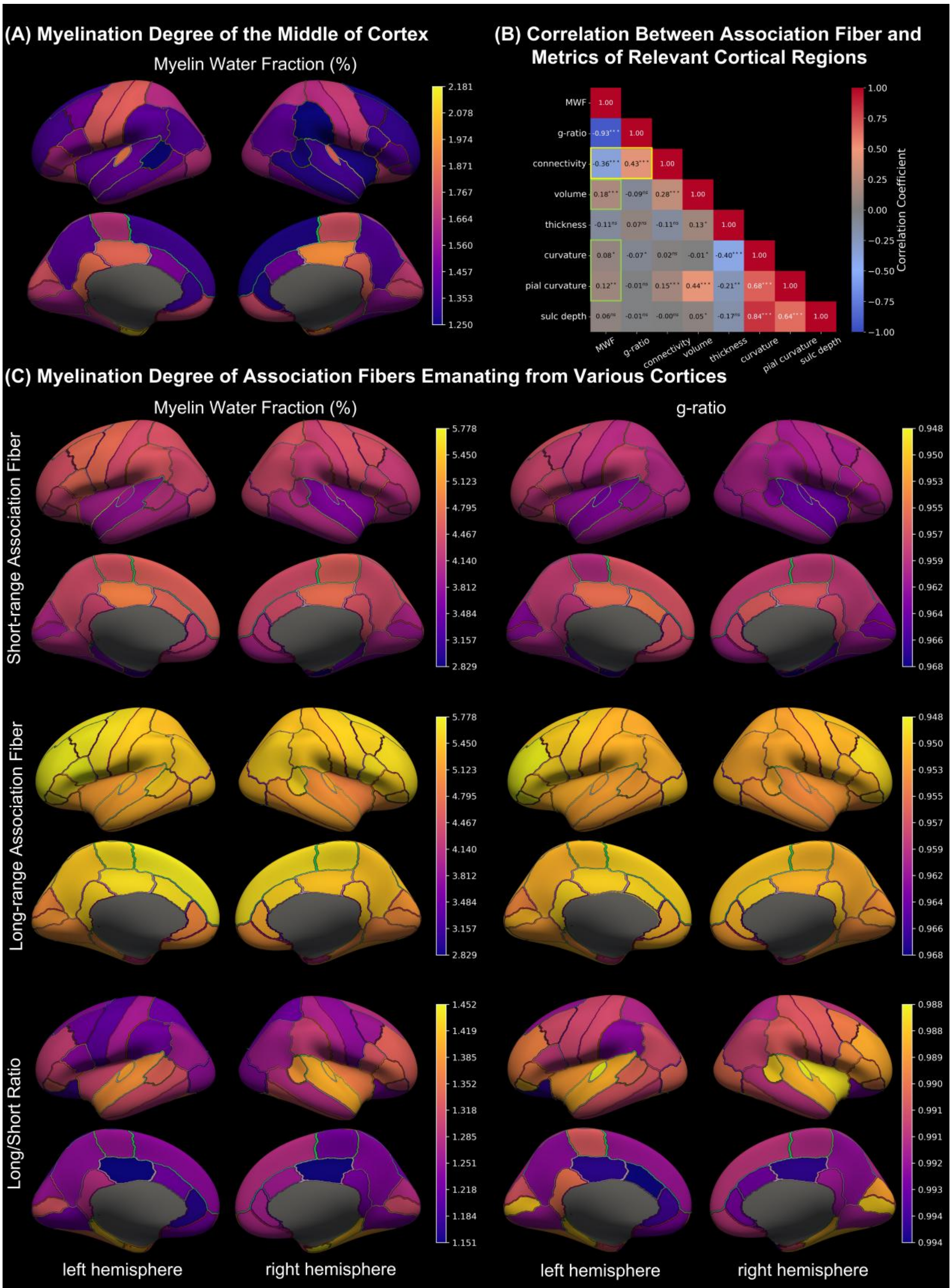

Figure 2. Analysis based on cortical regions and association fibers. (A) Expand the gray-white matter interface by half of the cortical thickness to obtain the cortices in the middle of the gray matter, projecting the MWF onto these cortices, and average the MWF values within the vertices of the brain regions to obtain the distribution of MWF across different brain areas. (B) Calculate the correlation index for the MWF and g-ratio of association fibers and related parameters of the two connected brain regions. (C) Plot the average values of MWF and g-ratio, for SAFs and LAFs originating from various brain regions, as well as the ratio of them.